2011

Direct numerical simulations of ignition of a lean n-heptane/air mixture with temperature inhomogeneities at constant volume: Parametric study

Chun Sang Yoo
Ulsan National Institute of Science and Technology (UNIST), Ulsan, Republic of Korea

Tianfeng Lu
University of Connecticut, Storrs, CT

Jacqueline Chen
Sandia National Laboratories, jhchen@sandia.gov

Chung K. Law
Princeton University, cklaw@princeton.edu

Combustion and Flame 158 (2011) 1727–1741

Contents lists available at ScienceDirect

Combustion and Flame

journal homepage: www.elsevier.com/locate/combustflame

Direct numerical simulations of ignition of a lean *n*-heptane/air mixture with temperature inhomogeneities at constant volume: Parametric study

Chun Sang Yoo [a,*], Tianfeng Lu [b], Jacqueline H. Chen [c], Chung K. Law [d]

[a] School of Mechanical and Advanced Materials Engineering, Ulsan National Institute of Science and Technology (UNIST), Ulsan 689-798, Republic of Korea
[b] Department of Mechanical Engineering, University of Connecticut, Storrs, CT 06269, USA
[c] Combustion Research Facility, Sandia National Laboratories, Livermore, CA 94551-0969, USA
[d] Department of Mechanical and Aerospace Engineering, Princeton University, Princeton, NJ 08544, USA

ARTICLE INFO

Article history:
Received 12 October 2010
Received in revised form 17 January 2011
Accepted 30 January 2011
Available online 15 March 2011

Keywords:
HCCI
DNS
n-Heptane reduced mechanism
Thermal stratification
Auto-ignition
Chemical explosive mode analysis

ABSTRACT

The effect of thermal stratification on the ignition of a lean homogeneous *n*-heptane/air mixture at constant volume and high pressure is investigated by direct numerical simulations (DNS) with a new 58-species reduced kinetic mechanism developed for very lean mixtures from the detailed LLNL mechanism (H.J. Curran et al., Combust. Flame 129 (2002) 253–280). Two-dimensional DNS are performed in a fixed volume with a two-dimensional isotropic velocity spectrum and temperature fluctuations superimposed on the initial scalar fields. The influence of variations in the initial temperature field, imposed by changing the mean and variance of temperature, and the ratio of turbulence to ignition delay timescale on multi-stage ignition of a lean *n*-heptane/air mixture is studied. In general, the mean heat release rate increases more slowly with increasing thermal stratification regardless of the mean initial temperature. Ignition delay decreases with increasing thermal stratification for high mean initial temperature relative to the negative temperature coefficient (NTC) regime. It is, however, increased with increasing thermal fluctuations for relatively low mean initial temperature resulting from a longer overall ignition delay of the mixture. Displacement speed and Damköhler number analyses reveal that the high degree of thermal stratification induces deflagration rather than spontaneous ignition at the reaction fronts, and hence, the mean heat release rate is smoother subsequent to thermal runaway occurring at the highest temperature regions in the domain. Chemical explosive mode analysis (CEMA) also verifies that mixing counterbalances chemical explosion at the reaction fronts for cases with large temperature fluctuation. It is also found that if the ratio of turbulence to ignition delay timescale is short, resultant diminished scalar fluctuations cause the overall ignition to occur by spontaneous ignition. However, the overall effect of turbulence is small compared to the effect of thermal stratification. These results suggest that the critical degree of thermal stratification for smooth operation of homogeneous charge compression-ignition (HCCI) engines depends on both the mean and fluctuations in initial temperature which should be considered in controlling ignition timing and preventing an overly rapid increase in pressure in HCCI combustion.

1. Introduction

Homogeneous charge compression-ignition (HCCI) combustion prototype engines are being developed as an alternative to conventional gasoline spark-ignition (SI) and diesel compression-ignition (CI) engines. HCCI combustion under lean, dilute, high-pressure and low-temperature conditions has the potential to provide high diesel-like efficiency with very low nitrogen oxides (NO_x) and particulate emissions. At these conditions HCCI combustion is thought to occur primarily through volumetric auto-ignition, largely in the absence of flames, and hence, is primarily controlled by chemical kinetics of the fuel–air mixture. Hence, one of the key issues in the development of HCCI engines is how to control the ignition timing and the rate of pressure rise or heat release rate under a wide range of load conditions [1,2]. In particular, an excessive rate of pressure rise under high-load condition can result in engine knock, reducing the engine integrity and hence, must be avoided through careful engine design and operation.

Over the past decade, numerous experimental and numerical studies on HCCI combustion have been conducted. The influence of thermal stratification and equivalence ratio fluctuations on the characteristics of HCCI combustion has been extensively investigated by the engine research community [1–17]. In these studies,

* Corresponding author. Fax: +82 52 217 2309.
E-mail address: csyoo@unist.ac.kr (C.S. Yoo).

0010-2180/$ - see front matter © 2011 The Combustion Institute. Published by Elsevier Inc. All rights reserved.
doi:10.1016/j.combustflame.2011.01.025

thermal stratification was proposed as a means to spread out the rate of pressure rise under high-load conditions [1,3–9]. In the presence of large temperature fluctuations, auto-ignition first occurs in hotter mixtures and then spreads to the remaining charge sequentially, such that combustion does not occur simultaneously throughout the engine cylinder.

On the other hand, mixture inhomogeneity was proposed to enhance and stabilize the HCCI combustion under low-load conditions [10–14]. Enhanced combustion could be achieved for a low mean equivalence ratio if locally rich pockets are present, which burn hotter and provide heat and radicals to adjacent leaner mixtures, and hence, significantly increase combustion efficiency. In addition to the mixture inhomogeneity, delayed-fuel injection was also considered to further increase temperature and composition stratification from the mixing process [14,15]. Recently, spark-assisted HCCI combustion [16,17] was also proposed to improve combustion efficiency in low-load engine operation and to control ignition timing. In spark-assisted HCCI combustion, a spark-ignited flame ultimately leads to compression heating and subsequent auto-ignition of the leaner mixtures, and hence, both flame and auto-ignition can coexist during the engine operation.

Ignition characteristics of HCCI combustion were also elucidated by direct numerical simulations (DNS) with detailed chemical kinetics. Two-dimensional DNS of ignition of lean hydrogen/air mixtures with temperature inhomogeneities [18–20] revealed that, for sufficiently large temperature fluctuations, deflagrations occur rather than volumetric auto-ignition, and consequently, the rate of heat release is spread out as the deflagrations propagate through the mixture. The transition between the normal deflagration regime and the subsonic spontaneous ignition front propagation regime was identified originally by Zel'dovich [21], although one significant difference between his original theory and the DNS findings is that it is the instantaneous, rather than initial thermal gradient, that is the relevant criteria in distinguishing between combustion regimes.

In addition, the effect of flow strain on the transient auto-ignition of mixtures has been studied in various configurations. Liu et al. [22,23] investigated the auto-ignition of diluted *n*-heptane jet flowing against heated air at high pressures in a one-dimensional counterflow configuration with steady and unsteady impulsive strain rate. More recently, Bansal et al. [24] studied the response of auto-ignition of one-dimensional nonpremixed *n*-heptane/air counterflow subjected to harmonic flow oscillations. From two-dimensional DNS, Im et al. [25] studied the ignition of a hydrogen/air scalar mixing layer in a homogeneous turbulence, and Echekki and Chen [26] investigated auto-ignition of non-homogeneous hydrogen/air mixtures prescribed by a scalar spectrum in homogeneous turbulence. These studies show that strong turbulence leads to intense mixing rates or high strain rate inhibits ignition by dissipating heat and intermediate species from ignition kernels.

Experimental studies, however, can still provide limited information including overall pressure rise, concentrations of NO_x, CO, and unburnt hydrocarbon emissions, and two-dimensional line-of-sight chemiluminescence or planar images of select species. Detailed characterization of chemical reactions occurring inside an engine chamber is still elusive. Similarly, previous multi-dimensional DNS were performed only with the simplest chemistry, hydrogen-air, owing to the prohibitive computational cost. As such, the results of the DNS were not directly applicable to the design and operation of practical hydrocarbon-fueled engines, although fundamentals of hydrogen/air ignition at constant volume under HCCI conditions were elucidated.

Therefore, the objective of the present study is two-fold: (i) to understand the ignition characteristics of practical hydrocarbon/air mixtures under HCCI conditions, and (ii) to provide strategies to control the rate of heat release in HCCI combustion by performing two-dimensional parametric DNS, systematically varying two key parameters: (1) the initial mean and variance of the temperature, and (2) the ratio of the turbulence to ignition delay timescale. In this study *n*-heptane is adopted as a surrogate fuel for large hydrocarbon fuels which generally exhibit two-stage ignition under HCCI conditions. Note that *n*-heptane has been widely used as a primary reference fuel (PRF) to investigate the characteristics of HCCI combustion in many previous studies [27–31].

2. *n*-Heptane reduced mechanism

The present reduced mechanisms for *n*-heptane oxidation were developed from a 188-species skeletal mechanism derived with a two-stage directed relation graph (DRG) [32] from the detailed LLNL mechanism with 561 species and 2539 elementary reactions [33,34]. The reduction flow chart is shown in Fig. 1, similar to the integrated reduction outlined by Lu and Law [35]. Note that although the 52-species reduced mechanism [36] is sufficiently small for the present simulations, it was derived for mixtures with an equivalence ratio, ϕ, larger than 0.5 and hence, may not be suitable for very lean HCCI conditions. In the present study, mixtures as lean as $\phi = 0.2$ are considered in the reduction to obtain a reduced mechanism for HCCI simulations through the following procedure.

First, DRG-aided sensitivity analysis (DRGASA) [37,38] was applied to the 188-species skeletal mechanism and an 88-species skeletal mechanism with 387 elementary reactions was obtained (see Supplementary materials). Second, quasi-steady state approximations (QSSA) were applied to the 88-species skeletal mechanism to further reduce the number of transported species. Using a criterion based on computational singular perturbation (CSP) [39], 24 species were identified as globally valid QSS species (i.e., HCO, CH3O, CH3CO, CH3CHO, pC4H9, C2H5CO, C2H5O, C3H5O, C4H7O, C4H8OOH1-3, C3H2, CH2(s), nC3H7CO, C7H15-1, C7H15-2, C7H15-3, C7H15-4, C7H14OOH1-3, C7H14OOH2-3, C7H14OOH2-4, C7H14OOH3-2, C7H14OOH3-4, C7H14OOH3-5, and C7H14OOH4-2). The algebraic equations for the QSS species were approximated using the linearized QSSA algorithm, which was analytically solved with graph theory for high numerical efficiency and robustness [40]. Third, strongly correlated isomers were grouped with the isomer lumping method [35] to further reduce the number of species in the reduced mechanism. Three isomer groups were identified, resulting in a 58-species reduced mechanism; i.e., group 1: 55% C7H14-2, 45% C7H14-3, group 2: 40% C7H14OOH2-4O2, 40%, C7H14OOH3-5O2, 20% C7H14OOH4-2O2, and group 3: 15% nC7KET13, 35% nC7KET24, 35% nC7KET35, 15% nC7KET42. Note that the intra-group mass fraction of an isomer is identical to its intra-group mole fraction because the isomers in the same group have the same molecular weight. Fourth, the method of diffusive species bundling [41] was utilized to group the species into 14 diffusive groups to facilitate the evaluation of the mixture-averaged species diffusion. The 58-species reduced mechanism involves all the 387 elementary reactions in the 88-species skeletal mechanism, since no elementary reaction was further eliminated through QSSA and isomer lumping in the present reduction.

Although the 58-species reduced mechanism is already compact in size for two-dimensional DNS of HCCI combustion, the mechanism is still stiff because there are locally fast-reacting radicals that cannot be regarded as global QSS species. Such fast-reacting radicals induce short chemical timescales which require much shorter time-steps for explicit time integration than that determined by the convection timescale. Therefore, as the last step of the reduction procedure, the method of dynamic stiffness removal [36] was employed to eliminate the chemical timescales shorter than 10 ns, such that the integration time-step in the

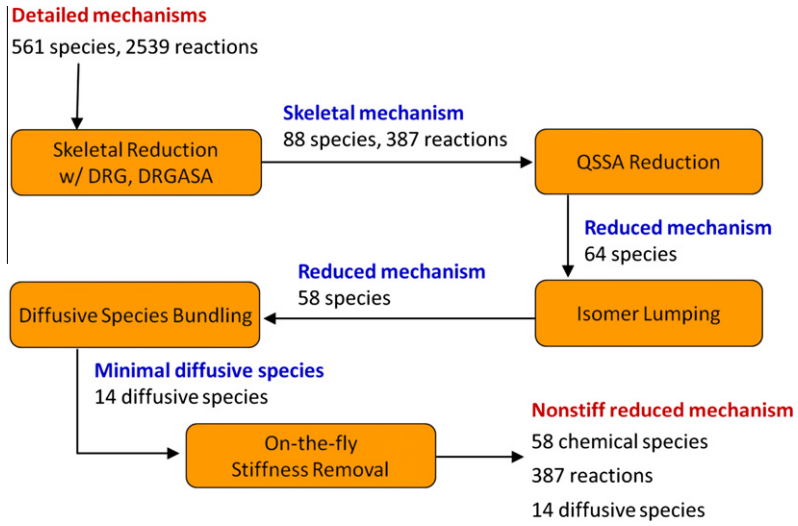

Fig. 1. Flow diagram illustrating the reduction procedure used to generate the 58-species *n*-heptane/air reduced mechanism.

present DNS is limited by the convection timescale represented by the CFL condition, rather than by the chemical stiffness.

The reduced mechanism was then validated with typical combustion applications including ignition, extinction, and flame propagation. Figure 2 shows the comparison of ignition delays at different equivalence ratios and pressures calculated with SENKIN [42] for auto-ignition under constant pressure. Note that, while both reduced mechanisms agree well with the detailed mechanism for equivalence ratio larger than 0.5, the accuracy of the 58-species mechanism is substantially improved compared with the 52-species mechanism at low temperatures for $\phi = 0.2$. Therefore, the 58-species reduced mechanism is suitable for HCCI problems for extremely lean mixtures. The 58-species reduced mechanism was further validated in perfectly stirred reactors (PSR). Figure 3 shows that the extinction time and temperature calculated with the reduced mechanism again agree well with those from the detailed mechanism. Finally, Fig. 4 shows the laminar flame speeds calculated using PREMIX code [43] with detailed and 58-species reduced mechanisms under 1 atm, and it is verified that the laminar flame speeds from the 58-species mechanism agree well with those from the detailed mechanism. This good agreement obtained from this test suite verifies the accuracy of the reduced mechanism

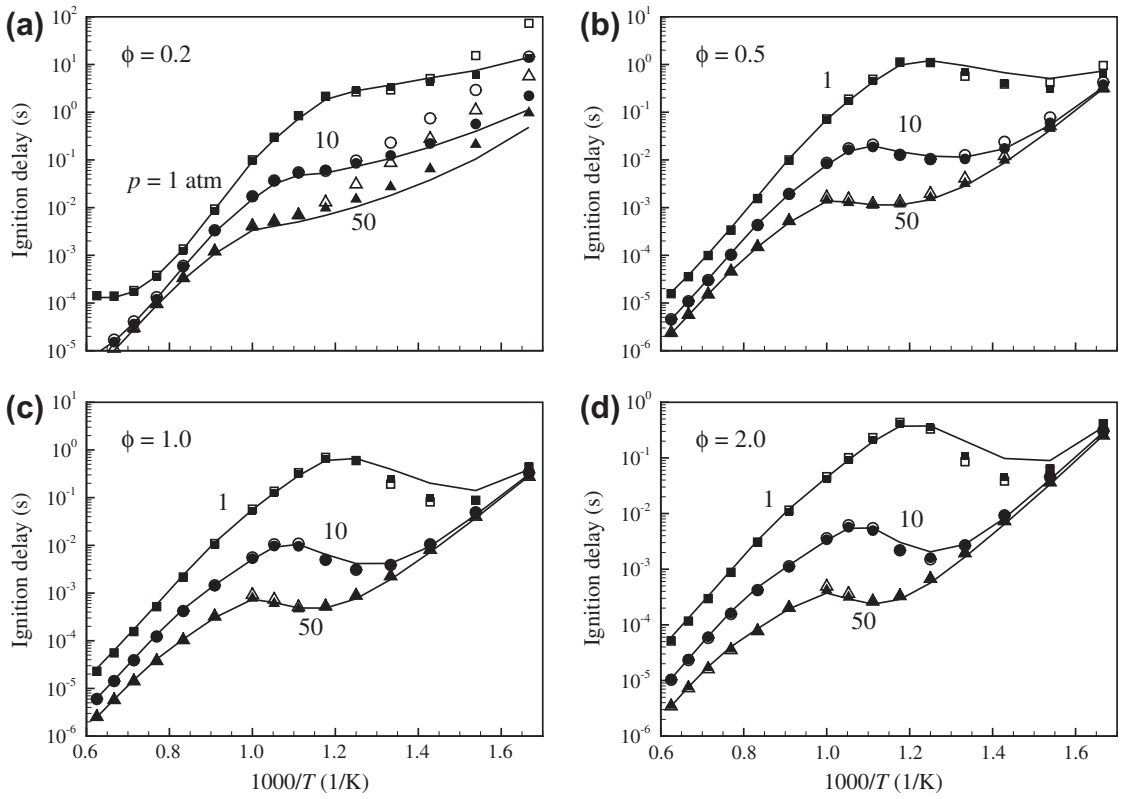

Fig. 2. Comparison of ignition delay versus initial temperature between detailed (line) [34], 58-species reduced (closed symbols), and 52-species reduced (open symbols) [36] mechanisms for *n*-heptane/air mixtures for various equivalence ratios at different pressures.

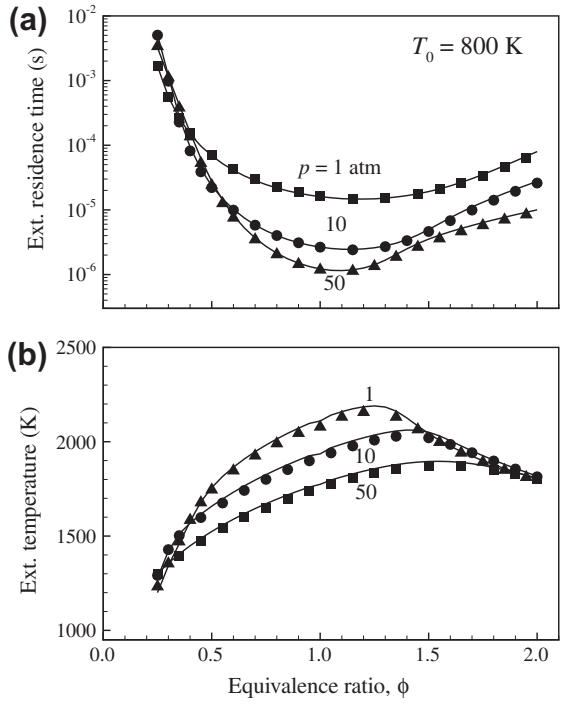

Fig. 3. Comparison of (a) extinction residence time and (b) extinction temperature versus equivalence ratio in PSR between detailed (lines) [34] and 58-species reduced (symbols) mechanisms for *n*-heptane/air mixtures at different pressures.

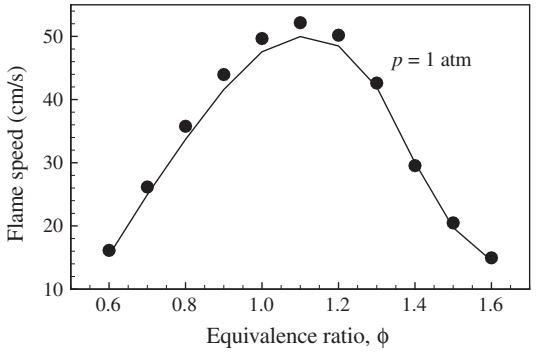

Fig. 4. Comparison of the laminar flame speed versus equivalence ratio between detailed (line) [34] and 58-species reduced (symbols) mechanisms for *n*-heptane/air flames at 1 atm.

for replicating HCCI conditions that may be encountered in DNS of turbulent compression ignition.

3. Numerical method and initial conditions

The compressible Navier–Stokes, species continuity, and total energy equations were solved using the Sandia DNS code, S3D [44]. A fourth-order explicit Runge–Kutta method by Kennedy and Carpenter [45] was used for time integration. The solution was spatially discretized using an eighth-order central differencing scheme. A tenth-order filter was employed to remove any spurious high-frequency fluctuations in the solution [46]. CHEMKIN and TRANSPORT software libraries [47,48] were linked with S3D to evaluate reaction rates and thermodynamic and mixture-averaged transport properties. Periodic boundary conditions were imposed in all directions such that ignition of a *n*-heptane/air mixture occurs at constant volume.

The initial uniform equivalence ratio, ϕ, and pressure, p_0, are 0.3 and 40 atm, respectively. Note that $\phi = 0.3$ is adopted to elucidate the ignition characteristics of a *n*-heptane/air mixture under relatively high-load conditions for HCCI engines [1,7]. Several parametric studies were performed to understand the effects of varying the initial mean and fluctuation of temperature and of varying the ratio of turbulence to ignition delay timescale. The initial turbulent flow field is prescribed by an isotropic kinetic energy spectrum function by Passot-Pouquet [49] as in [18,19,50,51]. The initial temperature field is also generated by a temperature spectrum, similar to the kinetic energy spectrum. Note that the two random fields are uncorrelated. For details regarding the generation of initial random fields, readers are referred to [19].

A total of 22 different DNS cases were performed in the parameter space of initial physical conditions: mean temperature T_0; temperature fluctuation root mean square (RMS) T'; most energetic turbulent length scale l_e; turbulence velocity fluctuation u'; turbulence timescale τ_t; and homogeneous ignition delay τ_{ig}^0. Henceforth, τ_{ig} represents the time at which the maximum mean heat release rate occurs, and the superscript 0 corresponds to the zero-dimensional simulation at constant volume. The most energetic length scale of the temperature fluctuation, l_{Te}, is 1.0 mm for all cases. Details of the physical and numerical parameters for the first 12 cases are presented in Table 1.

Note that in real HCCI engines, ignition delay is approximately 2 ms and turbulence timescale is $\sim O(1\text{ ms})$ [4,19,20]. The parameters in the present study were selected so that the turbulence timescale, $\tau_t = l_e/u'$, is comparable to the homogeneous ignition delay of the mixture at the same initial mean temperature and pressure, τ_{ig}^0, which significantly enhances turbulence-chemistry interaction. Also note that temperature fluctuations prior to the ignition in HCCI engines are approximately 15–20 K [14], which are much less than $T' = 60$ or 100 K for the present study. However, these high temperature fluctuations can be achieved through direct injection or delayed-fuel injection in HCCI combustion such that it is also important to understand the ignition characteristics of HCCI combustion with high T'.

The computational domain is a two-dimensional square box with each size of the domain, L, of 3.2 mm, discretized with $N = 640$ grid points for most cases. The corresponding grid resolution is 5.0 μm. This fine grid resolution is needed to resolve the ignition structure at high pressure. For several of the cases with large T' (i.e., Cases 4, 5, 9, and 12), 2.5 μm grid resolution is required to resolve thin flame-like structures. Typical profiles of initial temperature and vorticity in the DNS are shown in Fig. 5.

Note that while the integral scale of the temperature fluctuation in the DNS is typically smaller than that in a real engine, the length scale of the fluctuation does not control the evolution of the temperature gradient or its dissipation rate which controls the mode of

Table 1
Numerical and physical parameters of the DNS for different mean and RMS of initial temperature.

Case	T_0 (K)	T' (K)	l_e (mm)	u' (m/s)	τ_t (ms)	τ_{ig}^0 (ms)	L (mm)	N
1	850	7.5	1.24	0.5	2.49	2.49	3.2	640
2	850	15	1.24	0.5	2.49	2.49	3.2	640
3	850	30	1.24	0.5	2.49	2.49	3.2	640
4	850	60	1.24	0.5	2.49	2.49	3.2	1280
5	850	100	1.24	0.5	2.49	2.49	3.2	1280
6	934	15	1.24	0.5	2.49	2.49	3.2	640
7	934	30	1.24	0.5	2.49	2.49	3.2	640
8	934	60	1.24	0.5	2.49	2.49	3.2	640
9	934	100	1.24	0.5	2.49	2.49	3.2	1280
10	1008	15	1.24	0.5	2.49	2.49	3.2	640
11	1008	30	1.24	0.5	2.49	2.49	3.2	640
12	1008	60	1.24	0.5	2.49	2.49	3.2	1280

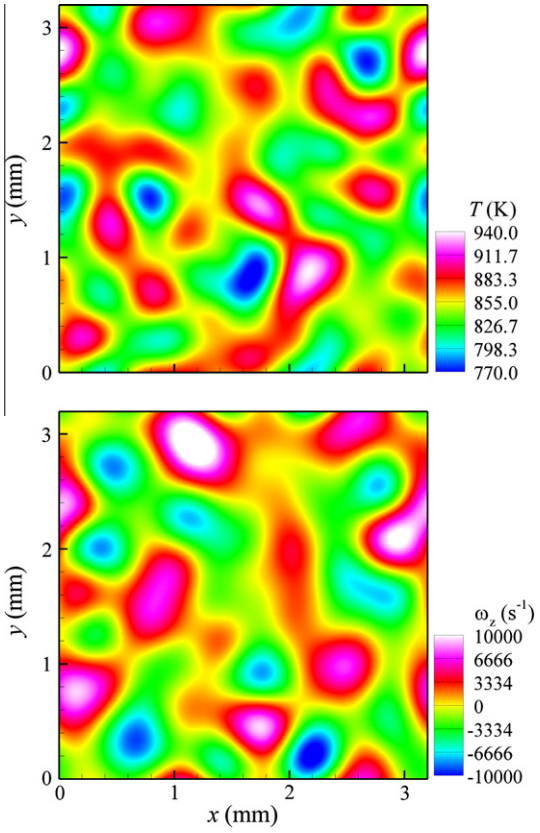

Fig. 5. Initial profiles of temperature and vorticity for Case 3 (T_0 = 850 K and T' = 30 K).

combustion. Assuming equilibrium between production and dissipation of thermal fluctuations, the thermal dissipation rate is proportional to the ratio of the temperature RMS to the turbulence timescale [52]. Hence, although the DNS integral length scales are smaller than those in an engine, as long as the turbulence timescale and temperature fluctuations are similar, the modes of combustion observed in the DNS will be relevant to modes in actual engines.

4. Effect of mean and RMS of initial temperature

In the first parametric study, the combined effect of mean and fluctuation of initial temperature on the ignition of a lean *n*-heptane/air mixture is investigated (see Table 1 for a description of detailed parameters). As discussed in Section 1, thermal stratification, achieved through either variations in mean or fluctuations in temperature, was proposed to prevent an excessive rate of pressure rise. Moreover, as the mean temperature of the engine chamber prior to thermal runaway can significantly change the ignition delay, it is expected that the effect of T' on the pressure rise can also be altered by the mean temperature of the fuel/air mixture. Therefore, three different initial mean temperatures near the negative temperature coefficient (NTC) regime were considered (i.e., T_0 = 850, 934, and 1008 K), all with identical homogeneous ignition delays $\left(\tau^0_{ig} = 2.49\ \text{ms}\right)$. The existence of the NTC regime is attributed to the transition of the ignition process from the low-temperature to intermediate-temperature chemistry. For details of *n*-heptane oxidation, readers are referred to [22,23,33,34,53]. Figure 6 shows τ^0_{ig} as a function of initial temperature. The first-stage ignition delay, $\tau^0_{ig,1}$, is also presented in the figure. While T_0 = 850 K and 934 K are within the NTC regime, T_0 = 1008 K is slightly outside of the NTC regime. Note also that two-stage ignition does not exist for T_0 > 940 K.

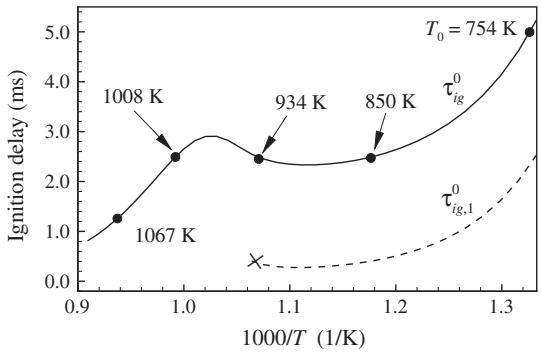

Fig. 6. Homogeneous ignition delay at constant volume with initial pressure of 40 atm as a function of initial temperature.

4.1. Overall combustion characteristics

For each mean initial temperature three to five DNS cases were performed with varying levels of temperature fluctuations, T'. Figure 7 shows the temporal evolution of mean heat release rate, $\bar{\dot{q}}$, for the cases. Three observations are noted from the figure. First, for the lower initial mean temperature cases with T_0 = 850 K (Cases 1–5), τ_{ig} is increased with increasing T'; on the contrary, for the higher initial mean temperature cases with T_0 = 1008 K, τ_{ig} is reduced with increasing T' (Cases 10–12). For T_0 = 934 K, τ_{ig} increases with small T', but decreases with large T'. Therefore, the cases with T_0 = 934 K exhibit the combined effects of low and high mean temperatures near the NTC regime. Second, for all cases as T' increases, $\bar{\dot{q}}$ is further spread out over time and the peak $\bar{\dot{q}}$ is reduced consistent with previous DNS of hydrogen/air ignition under HCCI conditions [20]. Third, the first-stage ignition delay for the cases with T_0 = 850 K is slightly decreased with T' and the corresponding peak $\bar{\dot{q}}$ is also reduced. There is, however, no significant difference in the first-stage ignition delays for the cases with T_0 = 934 K. Note also that first-stage ignition is negligible for cases with T_0 = 1008 K.

Figure 8 shows the temporal evolution of mean pressure and pressure rise rate. Since the mean pressure rise in current DNS at constant volume is solely attributed to temperature increase by heat release rate, the temporal evolution of pressure rise rate becomes nearly identical to that of heat release rate for each case. The rise of mean pressure is, thus, spread out more with increasing temperature RMS as shown in the figure. Note that the current DNS were performed at constant volume neglecting the piston motion in practical IC engines. This assumption may alter the combustion characteristics; i.e., the overall ignition timing may be reduced by isentropic compression heating during the early stage of ignition, and mixing may also be enhanced by turbulence generated by the piston wall. The effect of compression heating by a moving boundary in DNS on HCCI combustion is an ongoing research topic.

The dependence of $\bar{\dot{q}}$ on T_0 and T' is investigated by simply examining the initial temperature distributions of the DNS. The initial temperature distribution for each case spans a different range of ignition delays. Therefore, the overall ignition characteristics may be estimated from the initial distribution. Figure 9 shows the 95% range of τ^0_{ig} for initial mixtures with T' = 60 K for T_0 = 850, 934 and 1008 K (i.e., Cases 4, 8, and 12, respectively). The 95% range of τ^0_{ig} denotes the span of τ^0_{ig} in the initial mixture, wherein the corresponding temperature lies within 95% of the temperature range centered at the mean temperature. Note that small gaps between the lines in the figure are intentionally placed to clearly show the ranges. As shown in the figure, the range of τ^0_{ig}

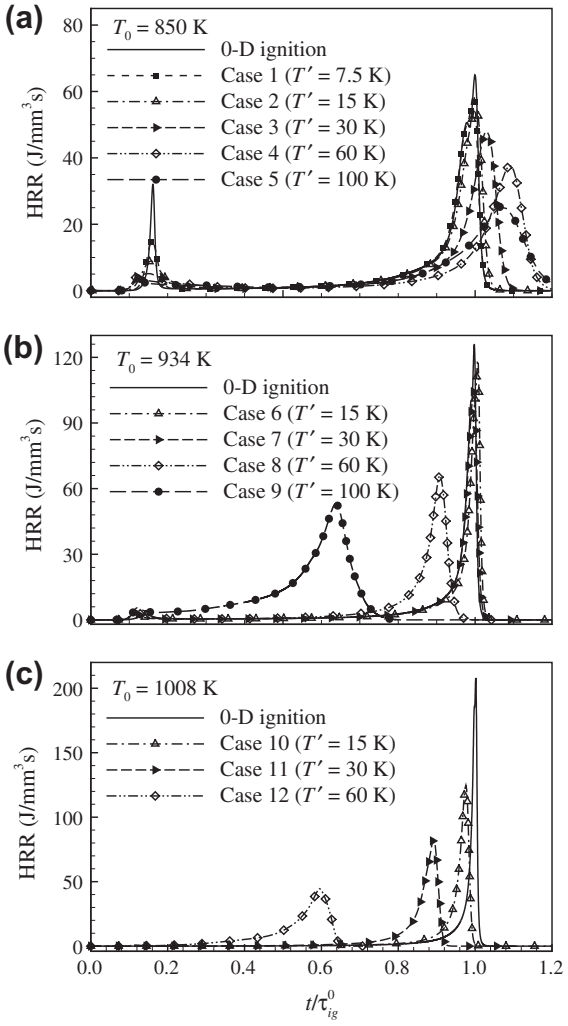

Fig. 7. Temporal evolution of mean heat release rate with different temperature RMS for (a) T_0 = 850, (b) 934, and (c) 1008 K.

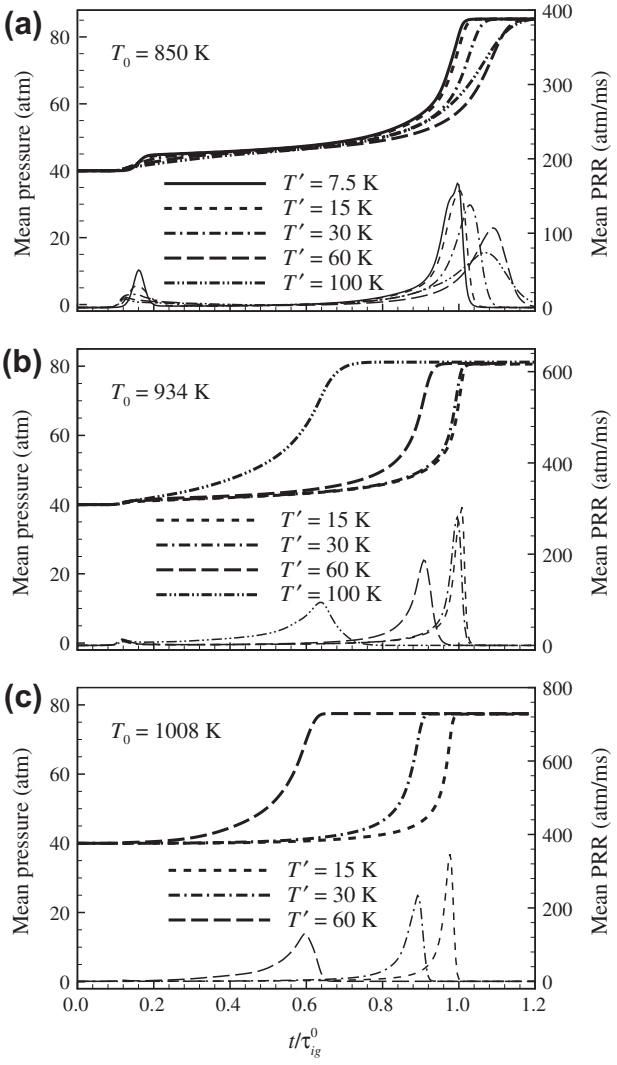

Fig. 8. Temporal evolution of mean pressure (thick lines) and pressure rise rate (thin lines) with different temperature RMS for (a) T_0 = 850, (b) 934, and (c) 1008 K.

for T_0 = 850, 934 and 1008 K are 2.33–7.18 ms, 1.57–2.90 ms, and 0.55–2.90 ms, respectively. Note that, for T_0 = 850 K (Case 4), the fastest ignition delay is comparable to the corresponding τ^0_{ig} (=2.49 ms) and the slowest ignition delay is three-times longer than τ^0_{ig}, much longer than the total time required for complete combustion (~3.0 ms, see Fig. 7a). Therefore, portions of the domain with long ignition delay significantly retard the overall combustion as shown in Fig. 7a.

On the contrary, for T_0 = 1008 K (Case 12), the fastest ignition delay is approximately five-times shorter than the corresponding τ^0_{ig}, such that the portions of the domain with short ignition delay accelerate the ignition progress over the homogeneous case, and hence, overall combustion occurs quickly. Note that, for T_0 = 934 K, T' = 100 K (Case 9) induces a similar degree of ignition enhancement as T' = 60 K (Case 12) with T_0 = 1008 K. Since T_0 = 934 K lies in the middle of the NTC regime, compared with T_0 = 1008 K cases, larger T' is required for the initial scalar field to include proportionately larger portions of the domain with higher initial temperature or shorter ignition delays. This simple estimate of the range of homogeneous ignition delays of mixtures shows that temperature fluctuations have a first-order effect on the ignition characteristics of *n*-heptane/air mixtures, with the sensitivities being greatest away from the NTC regime.

Hawkes et al. [20] found that deflagration due to large T' spreads out $\tilde{q}$ in the ignition of lean hydrogen/air mixtures. To verify this mechanism in the ignition of a *n*-heptane/air mixture, the overall structure of the heat release rate field is examined. Figure 10 shows isocontours of heat release rate, $\dot{q}$, for Cases 6–9 approximately at each τ_{ig}, normalized by the corresponding maximum heat release rate during the homogeneous ignition, $\dot{q}^0_m = 125.8$ J/mm^{3}s. It is readily observed from the figure that $\dot{q}$

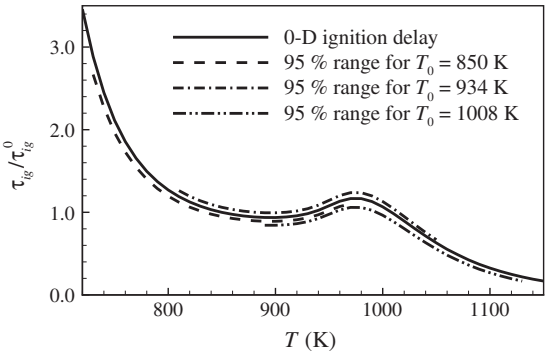

Fig. 9. The 95% range of ignition delay with T' = 60 K for DNS with T_0 = 850, 934, and 1008 K at initial pressure of 40 atm.

occurs nearly simultaneously throughout the domain as spontaneous ignition for small T' (Case 6). However, high $\dot{q}$ occurs primarily in thin sheets for large T' (Case 9), although relatively low $\dot{q}$ also occurs over a much broader area. Therefore, this suggests that the combustion mode is sensitive to variations with T'; i.e., the spontaneous ignition mode seems to be predominant for small T' while the mixed mode of deflagration and spontaneous ignition seems to occur for large T'.

Similarly, for Cases 5 and 12 with large T', ignition is advanced due to the existence of locally hotter mixtures, and $\bar{\dot{q}}$ is spread out more as shown in Fig. 7 since a significant fraction of the mixture with long ignition delays are likely to be consumed by deflagrations. Thus overall, combustion is controlled by flame propagation characteristics. A detailed analysis pertaining to the propagation and chemical characteristics of deflagration and spontaneous ignition modes is presented in the following sections.

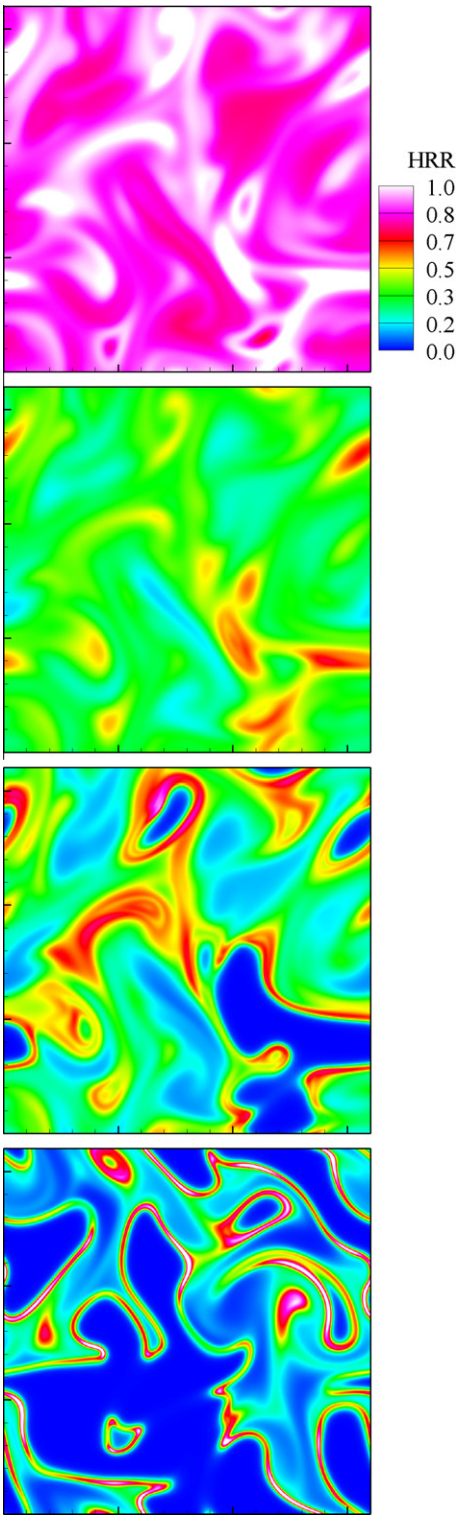

Fig. 10. Isocontours of normalized heat release rate for Cases 6–9 (from top to bottom) at t/τ_{ig}^0 = 1.0, 0.96, 0.88, and 0.60, respectively.

4.2. Combustion modes – propagation speed and burning rate

In this section, the nature of the combustion modes for the cases with different T_0 and T' is elucidated using diagnostics previously developed in [19,20]. Prior to examining the two-dimensional DNS cases, one-dimensional reference cases are simulated using a sinusoidal temperature profile. The wavelength of 1.24 mm in the one-dimensional cases matches the most energetic length scale, l_e, in the two-dimensional DNS cases and the mean and RMS temperature, T_0 and T', also match the two-dimensional DNS cases. Figure 11 shows the temporal evolution of temperature and heat release rate profile for T_0 = 934 K and T'=100 K corresponding to Case 9. Combustion progresses in the following manner: beyond the first-stage ignition (2–4 in Fig. 11), a high-temperature ignition kernel develops in the middle of the domain (5–7 in Fig. 11) and subsequently propagating combustion waves emanate, traveling to the left and right of the domain (8–10 in Fig. 11); finally, the remaining gas is heated by compression and consumed as the propagating combustion wave approaches the boundary of the domain (11 in Fig. 11). Combustion progresses nearly the same as for ignition of a lean hydrogen/air mixture [19], except for the addition of first-stage ignition. Note also that the presence of a propagating front does not necessarily imply that the front is a deflagration

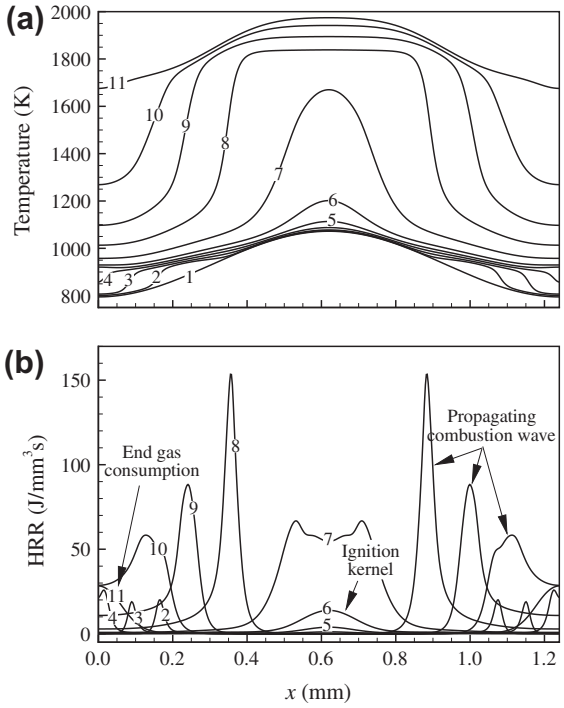

Fig. 11. Temporal evolution of (a) temperature and (b) heat release rate profiles with T_0 = 934 K and T' = 100 K. The equally spaced time sequence is numbered from 1 to 11, starting at 0.2 ms with an increment of 0.2 ms.

wave. The nature of the propagating wave and the role of molecular diffusion need to be identified.

For this purpose, the density-weighted displacement speed, S_d^*, is adopted to distinguish between deflagrations and spontaneous ignition fronts [19,20]. S_d^* is defined as [54–58]:

$$S_d^* = \frac{1}{\rho_u |\nabla Y_k|}\left(\dot{\omega}_k - \frac{\partial}{\partial x_j}(\rho Y_k V_{j,k})\right), \quad (1)$$

where Y_k, $V_{j,k}$, and $\dot{\omega}_k$ denote species mass fraction, species diffusion velocity in the j-direction and net production rate of species k, respectively, and ρ_u is the density of the unburnt mixture. ρ_u is calculated from the local enthalpy and fresh mixture condition assuming pressure and enthalpy remain constant across the front [19,20]. In the present study, the isocontour of $Y_c(\equiv Y_{CO_2} + Y_{CO}) = 0.04$ is chosen to evaluate the displacement speed. This particular isocontour coincides approximately with the location of maximum $\dot{q}$.

To understand the characteristics of propagating fronts in the simulations, it is necessary to compare S_d^* with the corresponding laminar flame speed, S_L. Note that unlike in the previous hydrogen/air DNS study [19], the laminar flame speed could not be obtained from a steady freely propagating flame computation using the PREMIX code [43] due to the highly reactive nature of the current n-heptane/air mixture. In this study, instead, the laminar flame speeds were estimated from transient one-dimensional reactive simulations. The simulations were initialized with a high-temperature ignition source such that a combustion wave emanates from the source, propagating into the reactive mixture ahead of it. Since auto-ignition in the reactive mixture does not occur prior to τ_{ig}^0, the speed of the propagating combustion wave, S_d^*, can be regarded approximately as the laminar burning velocity, S_L, at the corresponding pressure, similar to the diffusive limit found in the earlier hydrogen/air DNS study [19]. From the simulations, S_L of T_0 = 850, 934, and 1008 K are found to be approximately 0.2, 0.25, and 0.32 m/s, respectively. Note that these speeds do not change much with variations in the strength of the ignition source and the variation of the laminar flame speed with pressure is also less than 10% of mean values. Therefore, henceforth the laminar flame speeds described above provide a reference for comparison with S_d^*.

Figure 12 shows the temporal evolution of the front speed, S_d^*, for the one-dimensional laminar cases with different T_0 and T' corresponding to all of the two-dimensional DNS cases. Nominally, the curves exhibit a characteristics 'U' shape, also observed in previous studies [19,20]. Consistent with the two-dimensional DNS cases, overall combustion is advanced with increasing T' for cases with T_0 = 934 and 1008 K, but retarded for cases with T_0 = 850 K. Note also that, for all cases, during incipient thermal runaway, S_d^* of the nascent ignition kernel is significantly larger than the laminar flame speed, S_L. S_d^* is unbounded in the nascent ignition kernel since the scalar gradient, $|\nabla Y_k|$, in Eq. 1 vanishes [20,57]. Similarly, burnout of the remaining charge results in an abrupt thermal runaway due to compression heating, and thus, S_d^* is also unbounded there as shown in Fig. 11. Between the two singularities in S_d^*, however, deflagration of relatively constant speed is predominant for cases with large T', and hence, S_d^* exhibits values close to S_L with increasing T'.

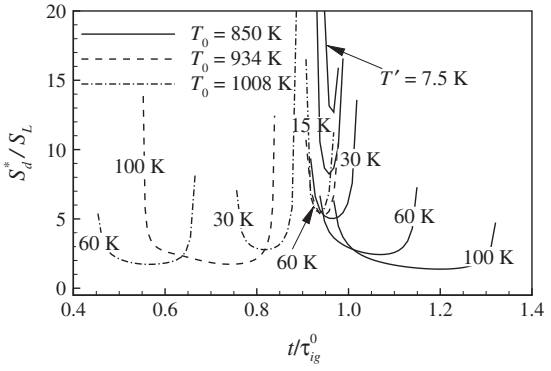

Fig. 12. Temporal evolution of the front speed, S_d^*, of one-dimensional reference cases with different T_0 and T'.

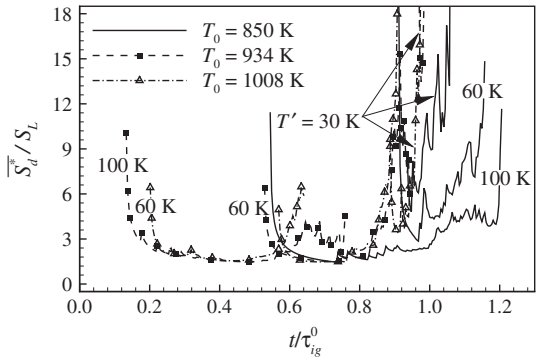

Fig. 13. Temporal evolution of the mean front speed, $\overline{S_d^*}$, for two-dimensional DNS cases with different T_0 = 850, 934, and 1008 K and T' = 30, 60, and 100 K.

Figure 12 also shows that the duration of the region of constant speed at the bottom of the 'U' shape increases with increasing T', suggesting that combustion at the reaction waves occurs primarily by deflagration rather than by spontaneous ignition. On the contrary, for cases with small T', the front speed is much greater than S_L to the extent that, for some cases, it is too large to be shown in Fig. 12 (e.g., T_0 = 934 K and T' = 15 K). Therefore, a small degree of thermal stratification leads an excessive rate of heat release due to simultaneous auto-ignition occurring throughout the whole domain, which should be avoided in HCCI combustion. These results also suggest that the critical degree of thermal stratification for smooth operation of HCCI engines depends on the mean initial temperature T_0, and hence, both initial T_0 and T' need to be considered to curtail too large a pressure rise rate.

The temporal evolutions of the mean front speed, $\overline{S_d^*}$, for the two-dimensional DNS cases is presented in Fig. 13. Note that the mean front speeds also exhibit a characteristic 'U' shape qualitatively similar to the corresponding one-dimensional cases. Comparison between Figs. 10 and 13 verifies that deflagration waves develop past initial thermal runaway for the cases with large T' as in the one-dimensional cases. Moreover, deflagration waves appear earlier and persist longer than the corresponding one-dimensional cases, simply because the large T' results in locally hotter mixtures than are present in the one-dimensional cases, and hence, locally auto-ignition can occur and evolve into a deflagration wave sooner than in the one-dimensional cases.

A quantitative measure of the occurrence of deflagration and spontaneous ignition modes in the combustion process is obtained from the temporal evolution of the fraction of heat release rate occurring in the deflagration mode for the two-dimensional DNS data as shown in Fig. 14. To distinguish between the two modes of propagation, the Damköhler number, Da, defined by [26,58,59], is adopted:

$$Da = \frac{\dot{\omega}_k}{|-\partial(\rho Y_k V_{j,k})/\partial x_j|}, \quad (2)$$

where $Y_c(= Y_{CO_2} + Y_{CO})$ is used to evaluate Da. From one-dimensional laminar simulations, it is found that Da in the diffusive limit is approximately 4.0. The departure from unity is because, although the combustion wave propagates under the diffusive limit, the upstream mixture is highly reactive and hence, the reaction

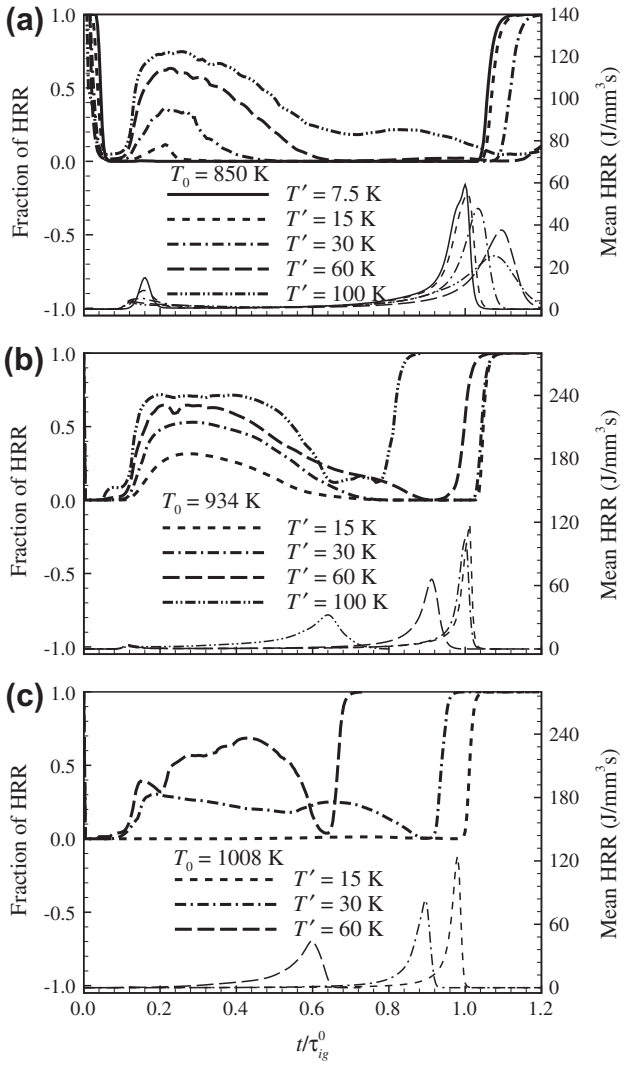

Fig. 14. Temporal evolution of fraction of heat release rate from the deflagration mode (thick lines) and heat release rate (thin lines) with different temperature RMS for (a) T_0 = 850, (b) 934, and (c) 1008 K.

term is somewhat larger than the diffusion term. In the present study, the delineation between the two propagation modes is defined by *Da* less than 4.0 (deflagration wave).

Several observations can be made from Fig. 14. First, at the initial and final stages of the ignition, the fraction of $\dot{q}$ from the deflagration mode becomes unity simply because the corresponding reaction rate vanishes, and thus, *Da* also vanishes. Second, the fraction of $\dot{q}$ from the deflagration mode increases with increasing T', such that over half of the heat release rate occurs in the deflagration mode between the first- and the second-stage ignition for cases with large T'. Third, for small T', the fraction of $\dot{q}$ from the deflagration mode vanishes much sooner than the occurrence of the peak $\bar{\dot{q}}$; on the contrary, for large T' (i.e., Cases 5, 9, and 12), a considerable fraction of $\dot{q}$ still occurs in the deflagration mode at the point when $\bar{\dot{q}}$ peaks. As discussed earlier in reference to the one-dimensional laminar cases, at the final stage of ignition, the remaining unburned charge is heated by compression and consumed as simultaneous ignition, exhibiting large values of S_d^*. Therefore, only a small fraction of combustion occurs in the deflagration mode during the final stages of ignition, verifying that spontaneous auto-ignition occurs for small T'. However, a relatively large fraction of the deflagration mode with large T' indicates the occurrence of mixed modes of deflagration and spontaneous ignition. These results, further, verify that deflagration is attributed to spreading out the heat release rate.

The occurrence of the deflagration mode is further identified by examining the probability density functions (PDF) of S_d^* for the two-dimensional cases as shown in Fig. 15. The PDFs were constructed using all of the data for each case. In general, the peak of the PDF shifts to a smaller value with increasing T'. It is also found that, for small T', the PDF spans a wide range of front speeds with low probability, typically larger than S_L. On the contrary, for large T', the PDF is narrow in extent, with high probability at low front speeds. This result together with mean front speed shown in Fig. 13 verifies that the reaction fronts occur primarily as deflagration waves for large T'.

4.3. Chemical explosive mode analysis

Chemical explosive mode analysis (CEMA) was recently developed for systematic detection of critical flame features such as ignition, extinction, and premixed flame fronts [60,61]. CEMA is based on eigen-analysis of the Jacobian matrix of the chemical source terms in the species and energy equations, and hence, a chemical mode associated with a positive eigenvalue indicates an explosive mixture that, in isolation, would lead to ignition. Such explosive mixtures are typically observed in the radical explosion and thermal runaway stages of auto-ignition and in the preheat

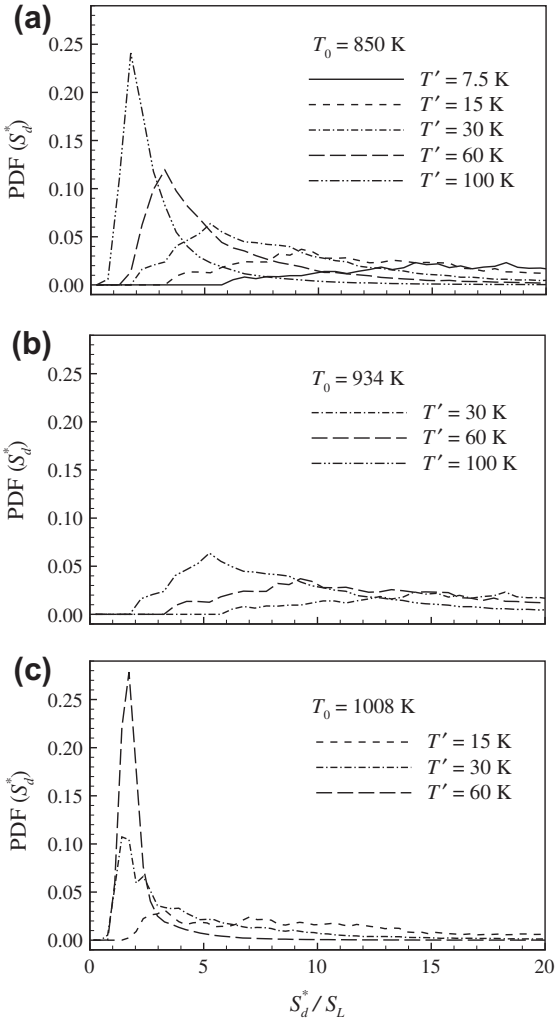

Fig. 15. The PDF of the front speed, S_d^*, for two-dimensional DNS cases with different T_0 and T': (a) T_0 = 850, (b) 934, and (c) 1008 K.

zones of premixed flames. Chemical explosive modes (CEM) are also important for flame extinction as discussed by Lu et al. [61]. As such, in the present study, to further identify the characteristics of combustion waves of *n*-heptane/air mixtures under HCCI conditions, CEMA together with the local scalar dissipation rate is adopted to account for losses due to turbulent mixing. CEMA is also employed to distinguish pre- and post-ignition mixtures and to pinpoint the location of the ignition fronts in the DNS cases.

Two cases (i.e., Cases 6 and 9 in Fig. 10) were selected for CEMA because of their distinctive ignition processes. Figure 16 shows the isocontours of the timescale of the CEM, Damköhler number, temperature, and scalar dissipation rate for Case 6 (T_0 = 934 K and T' = 15 K) at $t/\tau_{ig}^0 = 1.0$. The timescale of the CEM is the reciprocal eigenvalue, λ_{exp}, of the CEM as shown in Fig. 16a, where red indicates explosive or unburned mixtures, and blue indicates non-explosive or burned mixtures. The sharp boundaries separating the burned and unburned mixtures are the reaction fronts that can be either spontaneous ignition or a deflagration wave. Figure 16b shows alternative definition of Damköhler number based on the product of the timescale of the CEM and the scalar dissipation rate, χ_c [59,60]:

$$Da_c = \lambda_{exp} \cdot \chi_c^{-1}, \tag{3}$$

where χ_c is defined by $\chi_c = 2D|\nabla c|^2$. Note that the progress variable, c, is given by $c \equiv Y_c/Y_c^{Eq}$, where Y_c^{Eq} is the corresponding equilibrium value of $Y_c (= Y_{CO_2} + Y_{CO})$, and D is the thermal diffusivity of the local mixture. The solid lines are the ignition fronts extracted from Fig. 16a. Figure 16c and d shows temperature and scalar dissipation rate fields together with the ignition fronts, respectively.

Note that a large positive value of Da_c (red) in Fig. 16b indicates that the chemical explosive process dominates the mixing process and, as such, the mixture is auto-igniting. On the other hand, a large negative value of Da_c (blue) indicates a highly reactive post-ignition (burned) mixture, where fast chemistry is exhausted and rate-limited by mixing. It is readily observed from Fig. 16b that the entire domain is composed of two bulk regions; i.e., the auto-igniting (red) and the post-ignition (blue) regions, respectively, separated by the thin reaction fronts. It can also be observed that Da_c upstream of the combustion waves are much larger than unity, suggesting that the chemical reaction represented by λ_{exp} is also much faster than the mixing process represented by χ_c. In general, the reaction and diffusion terms counterbalance each other in deflagration waves, resulting in Da of order of unity. Ahead of the reaction fronts, however, values of Da much larger than unity can be observed in Fig. 16b, indicating that the latter are attributed to spontaneous ignition rather than deflagration. Note that the temperature difference upstream and downstream of the reaction fronts in Fig. 16c is relatively small, which is not the case for a normal deflagration wave, also suggesting that the reaction fronts are spontaneous ignition fronts.

It is also of interest to note that, while temperature is high in post-ignition zones, the igniting mixtures, such as those undergoing

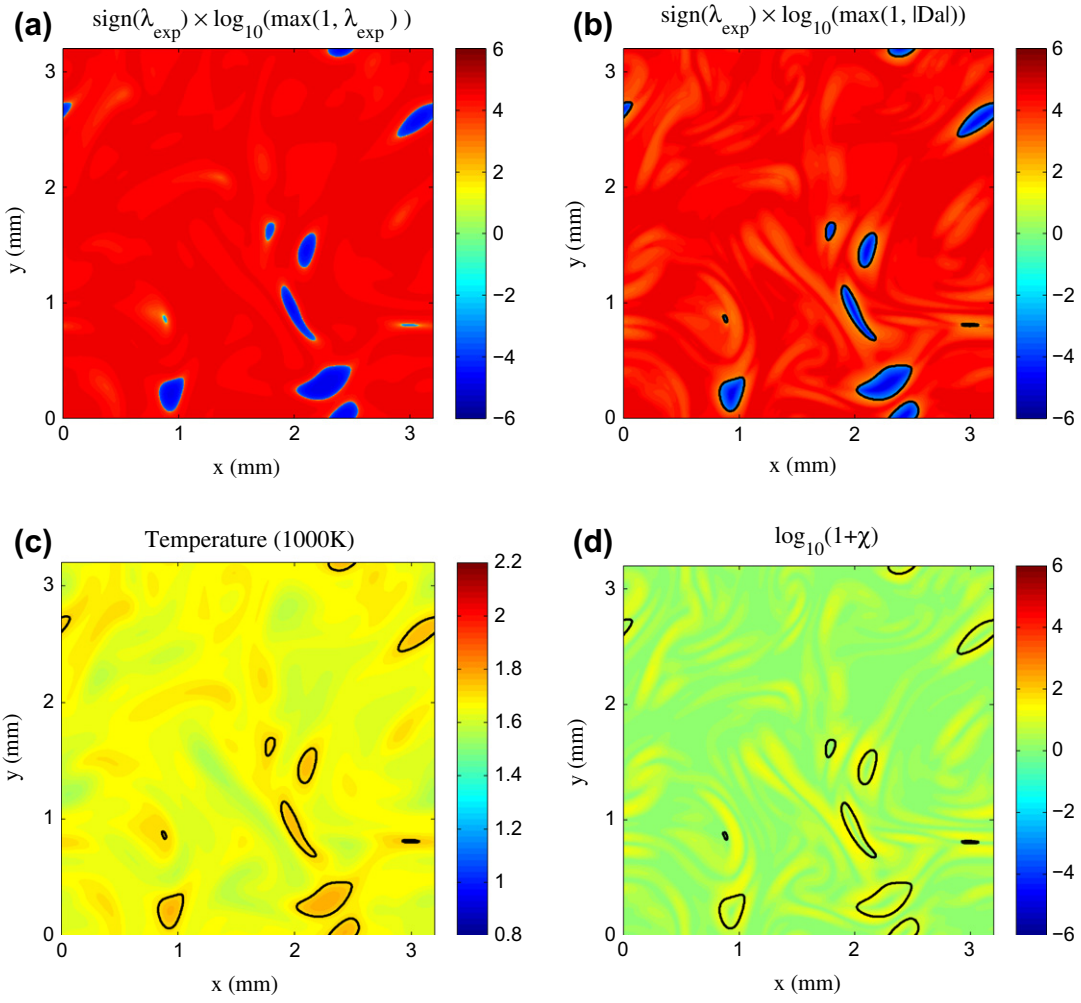

Fig. 16. Isocontours of (a) timescale of chemical explosive mode, (b) Damköhler number, (c) temperature, and (d) scalar dissipation rate for Case 6 (T_0 = 934 K and T' = 15 K) at $t/\tau_{ig}^0 = 1.0$. The solid line denotes the ignition front.

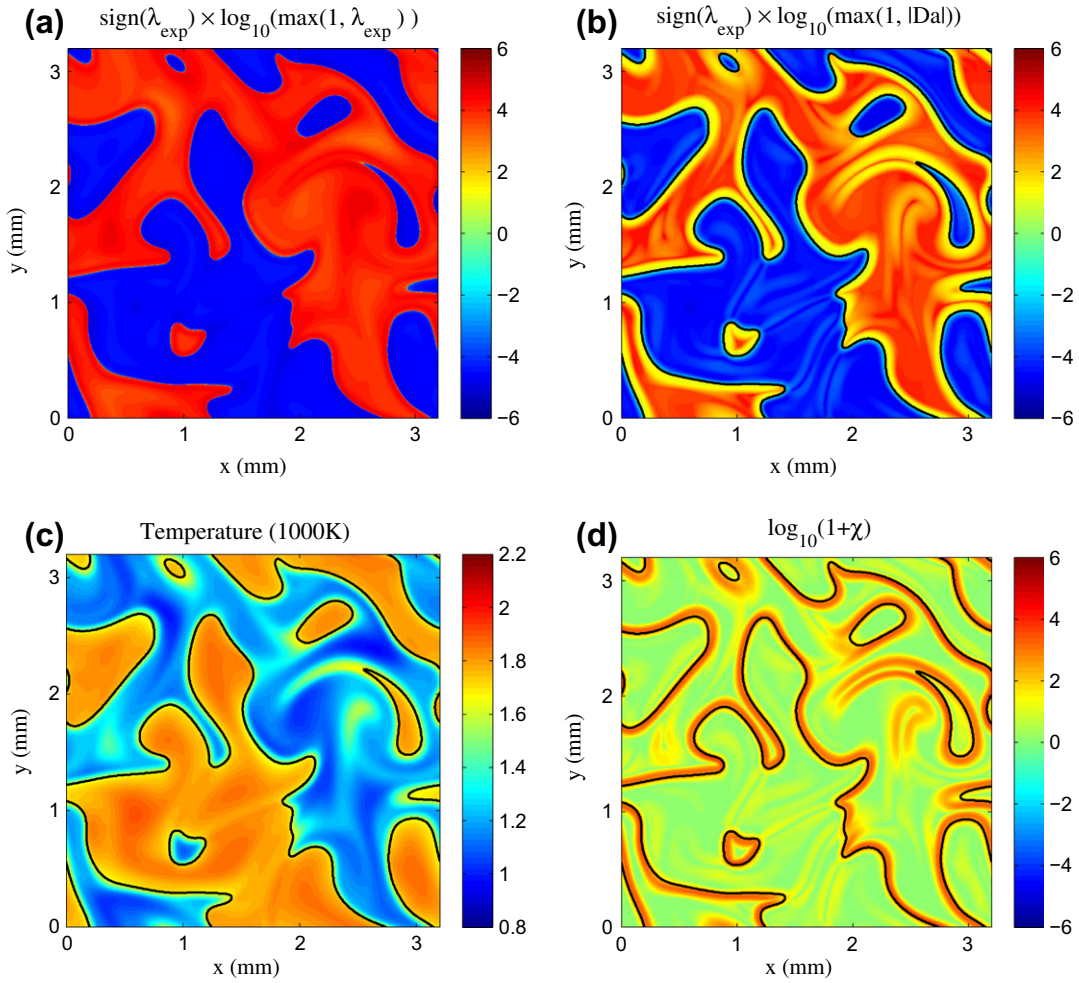

Fig. 17. Isocontours of (a) timescale of chemical explosive mode, (b) Damköhler number, (c) temperature, and (d) scalar dissipation rate for Case 9 (T_0 = 934 K and T = 100 K) at $t/\tau_{ig}^0 = 0.6$. The solid line denotes the ignition front.

thermal runaway, may also exhibit moderately high temperatures, and hence, the reaction fronts are difficult to determine only based on temperature. Similarly, scalar dissipation rates may peak near the reaction fronts or in auto-igniting zones such that the reaction fronts may not be clearly identified by the scalar dissipation rate. Therefore, CEM is a better indicator than temperature and scalar dissipation rate in classifying the pre- and post-ignition mixtures.

Figure 17 shows the isocontours for Case 9 (T_0 = 934 K and T = 100 K) at $t = \tau_{ig}$. It is readily observed from Fig. 17b that there exist three bulk regions; the auto-igniting region (red), the post-ignition region (blue), and the yellow-greenish region where mixing balances chemical explosion. As the mixing represented by χ_c exhibits the same order of magnitude as the chemical explosion represented by λ_{exp}, the corresponding Da_c upstream of the reaction fronts becomes order of unity as shown in the figure. This result verifies that the reaction fronts of Case 9 are deflagration waves rather than spontaneous ignition fronts as explained in the previous section. The mixtures encompassed by the deflagration waves in Fig. 17c mostly feature higher temperatures and those outside the ignition fronts exhibit lower temperature, which coincides with the structure of a normal deflagration wave. Figure 17d further shows that the ignition fronts mostly overlap with the strips with large χ_c, a feature of deflagration waves propagating through unburned mixtures prior to the occurrence of auto-ignition.

4.4. High and low initial mean temperatures

To understand the effect of different ignition delays on the ignition characteristics, two additional initial mean temperatures are also investigated. Six additional DNS were performed with high (T_0 = 1067 K) and low (T_0 = 754 K) mean temperatures such that their corresponding homogeneous ignition delays are 1.24 ms and 4.98, respectively. Readers are referred to Table 2 for the physical parameters of these cases.

Figure 18 shows the temporal evolution of $\bar{\dot{q}}$ with different T for T_0 = 1067 K (Cases 13–15) and 754 K (Cases 16–18). For high T_0 compared with the NTC regime, ignition occurs in a single stage similar to ignition of a lean hydrogen/air mixture [20] and to the *n*-heptane case with T_0 = 1008 K (Cases 10–12). Therefore, the effect of thermal stratification on the ignition characteristics for the cases with T_0 = 1067 K is also similar to those for a lean hydrogen/air mixture and the *n*-heptane case with T_0 = 1008 K; i.e., as T increases, the ignition delay decreases and the mean heat release rate spreads out more. For cases with T_0 = 754 K, however, the ignition delay and spreading of $\bar{\dot{q}}$ are not significantly affected by thermal stratification. For these cases, τ_t (=2.49 ms) is much shorter than τ_{ig}^0 (= 4.98 ms) such that turbulent straining and mixing homogenize any thermal stratification prior to second-stage ignition. Hence, second-stage ignition is not significantly affected unlike first-stage ignition, which is remarkably altered by T. The

Table 2
Numerical and physical parameters of the DNS for high and low initial mean temperatures.

Case	T_0 (K)	T' (K)	l_e (mm)	u' (m/s)	τ_t (ms)	τ_{ig}^0 (ms)	L (mm)	N
13	1067	15	1.24	0.5	2.49	1.24	3.2	640
14	1067	30	1.24	0.5	2.49	1.24	3.2	640
15	1067	60	1.24	0.5	2.49	1.24	3.2	1280
16	754	15	1.24	0.5	2.49	4.98	3.2	640
17	754	30	1.24	0.5	2.49	4.98	3.2	640
18	754	60	1.24	0.5	2.49	4.98	3.2	1280

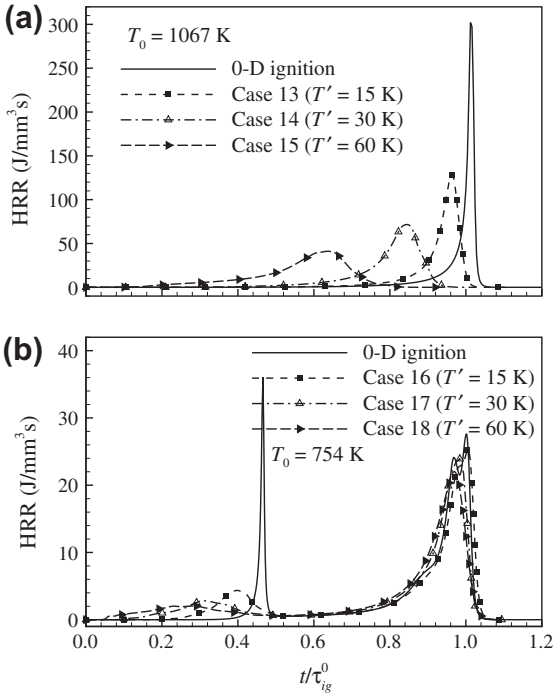

Fig. 18. Temporal evolution of mean heat release rate for different T' for (a) T_0 = 1067 K and (b) T_0 = 754 K.

effect of the ratio of turbulence timescale to ignition delay is further investigated in the next section.

The ignition characteristics for the cases with high and low T_0 are further investigated by examining their mean front speeds as shown in Fig. 19. For cases with T_0 = 1067 K, $\overline{S_d^*}$ exhibits a characteristics 'U' shaped behavior with large T' similar to the cases with intermediate T_0 and the duration of deflagration becomes longer with increasing T', suggesting that deflagration becomes dominant at the reaction fronts with high T_0 and large T', consistent with the intermediate mean temperature cases. However, for cases with low T_0 (=754 K), the mean front speeds do not exhibit a characteristic 'U' shape since the predominant combustion mode for these cases is simultaneous auto-ignition induced by temperature homogenization due to fast turbulent mixing. Therefore, the resultant mean front speed has a much larger value than the corresponding laminar flame speed.

5. Effect of ratio of turbulence to ignition delay timescale

The effect of turbulence timescale on the ignition characteristics of a lean *n*-heptane/air mixture is also investigated. To understand competitive effects of turbulence timescale and T' on the ignition characteristics, two specific sets of T_0 and T' (T_0 = 850 K and

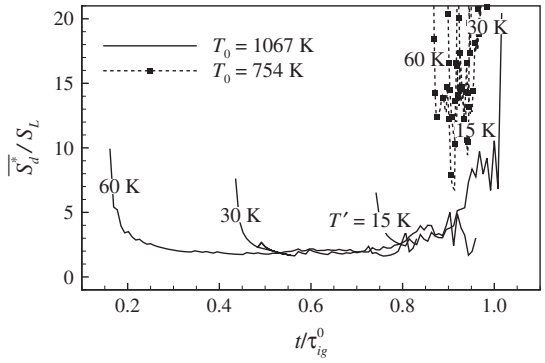

Fig. 19. Temporal evolution of the mean front speed $\overline{S_d^*}$ for two-dimensional DNS cases for T_0 = 1067 and 754 K with different T'.

Table 3
Numerical and physical parameters of the DNS for different turbulence timescale.

Case	T_0 (K)	T' (K)	l_e (mm)	u' (m/s)	τ_t (ms)	τ_{ig}^0 (ms)	L (mm)	N
2	850	15	1.24	0.5	2.49	2.49	3.2	640
19	850	15	0.96	2.0	0.48	2.49	6.4	1280
20	850	15	3.91	0.3	13.0	2.49	6.4	1280
9	934	100	1.24	0.5	2.49	2.49	3.2	1280
21	934	100	0.96	2.0	0.48	2.49	3.2	1280
22	934	100	3.91	0.3	13.0	2.49	3.2	1280

T' = 15 K; T_0 = 934 K and T' = 100 K) and three turbulence timescales (τ_t = 0.48, 2.49, and 13.0 ms) were selected such that four additional DNS were performed (see Table 3). The cases are compared with Cases 2 and 9 in which τ_t is 2.49 ms with identical T_0 and T'. The corresponding ratios of turbulence to homogeneous ignition delay, τ_t/τ_{ig}^0, are 0.2, 5.2, and 1.0.

The temporal evolution of $\bar{\dot{q}}$ is examined first as shown in Fig. 20. Several points are noted from the figure. For cases with T_0 = 850 K and T' = 15 K (Cases 2, 19, and 20), the overall characteristics of first-stage ignition are unaffected by the turbulence timescales, and τ_{ig} decreases and $\bar{\dot{q}}$ is more spread out with increasing τ_t as shown in Fig. 20a. After the first-stage ignition, the overall shape of $\bar{\dot{q}}$ for Case 19 with small τ_t is nearly identical to that of the homogeneous ignition except for the second ignition delay. Similarly, for cases with T_0 = 934 K and T' = 100 K (Cases 9, 21, and 22), $\bar{\dot{q}}$ is more spread out with increasing τ_t as shown in Fig. 20b. However, τ_{ig} first decreases and then increases with increasing τ_t. Moreover, short τ_t (Case 21) significantly increases τ_{ig} compared to longer τ_t (Cases 9 and 22) and its overall shape of $\bar{\dot{q}}$ is also similar to that of the homogeneous ignition except for the short second ignition delay. All of these ignition characteristics are attributed to the relative timescales between the ignition delay and turbulence timescales and the overall combustion modes.

To understand the mixing characteristics of flows with different turbulence timescales, the temporal evolution of T' is examined as shown in Fig. 21. For cases with T_0 = 850 K and T' = 15 K (Cases 2, 19, and 20), during first-stage ignition, T' for the three cases are similar since the turbulence timescales in the DNS are much larger or at least comparable to the first-stage ignition delay: i.e., there is insufficient time for the turbulence to homogenize the temperature fluctuations. After first-stage ignition, however, T' for Case 19 decreases below its initial value of 15 K, remaining nearly constant until second-stage ignition starts. On the contrary, T' for Case 20 remains larger than the other two cases and, in particular, the second peak of T' becomes much greater than the other cases. Therefore, a short turbulence timescale, τ_t, (Case 19) relative to

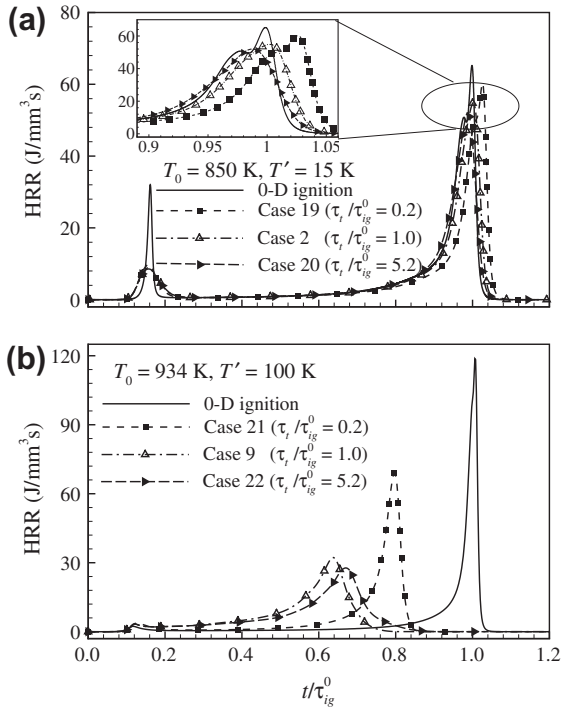

Fig. 20. Temporal evolution of mean heat release rate for different turbulence timescales for (a) T_0 = 850 K with T' = 15 K and (b) T_0 = 934 K with T' = 100 K.

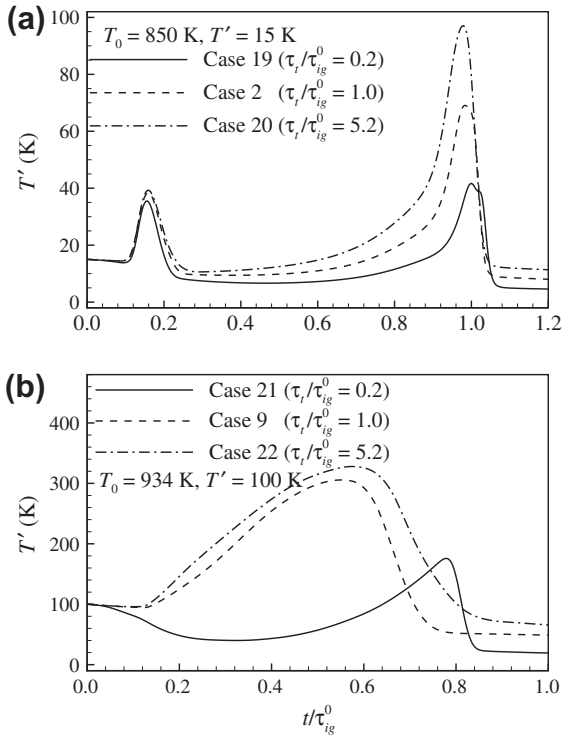

Fig. 21. Temporal evolution of temperature fluctuation RMS for different turbulence timescales for (a) T_0 = 850 K with T' = 15 K and (b) T_0 = 934 K with T' = 100 K.

the ignition delay homogenizes the temperature field quickly such that combustion is more apt to occur by spontaneous ignition although the ignition delay is increased by diminished extrema of T'. The net effect of a small ratio of turbulence to ignition delay timescale is to dissipate heat and radicals from ignition kernels [26], resulting in an increased τ_{ig} and $\bar{\dot{q}}$ profile similar to that of the corresponding homogeneous ignition (as shown in Fig. 21a comparing Case 19 with 0-D ignition). Turbulent flow with long τ_t (Case 20) is, however, unable to homogenize temperature fluctuations within the overall combustion timescale ($>\tau_{ig}$) such that ignition can occur independently in each ignition kernel, and hence, $\bar{\dot{q}}$ is more spread out as shown in Fig. 20a.

For cases with T_0 = 934 K and T' = 100 K (Cases 9, 21, and 22), only T' with short τ_t (Case 21) exhibits a similar second ignition delay behavior as those for cases with T_0 = 850 K (see Fig. 21b). Similar to Case 19, turbulent flow with short τ_t (Case 21) homogenizes the temperature field quickly such that combustion is more apt to occur by spontaneous ignition. For this case, however, the effect of large T' is more significant than that of short turbulence timescale, leading to the short ignition delay relative to τ_{ig}^0. For cases with longer τ_t (Cases 9 and 22), Figs. 14b and 17 imply that a significant fraction of the mixture is consumed by deflagration waves, resulting in the significant increase of T' beyond the first-stage ignition as shown in Fig. 21b. It is of interest to note that although overall T' values for Case 22 are greater than those for Case 9, τ_{ig} for Case 22 is longer relative to Case 9. Therefore, turbulent mixing seems to be able to enhance the overall combustion by inducing spontaneous ignition even in deflagration-dominant combustion.

To further identify this non-monotonic ignition delay behavior for cases with T_0 = 934 K and T' = 100 K, the fraction of $\dot{q}$ occurring in the deflagration mode is shown in Fig. 22. For Case 21 with short τ_t, the deflagration mode combustion is dominant between the first and the second ignition. However, the fraction of $\dot{q}$ from the deflagration mode nearly vanishes at the peak in heat release rate, similar to cases with small T' (see Figs. 14 and 22a). This verifies that short τ_t can induce spontaneous auto-ignition even for the case with large T'. For Cases 9 and 22, however, a considerable fraction of $\dot{q}$ still occurs in the deflagration mode at the point when $\bar{\dot{q}}$ peaks, verifying that spreading of $\bar{\dot{q}}$ is attributed to the deflagration mode of combustion. It is also observed from the figure that for

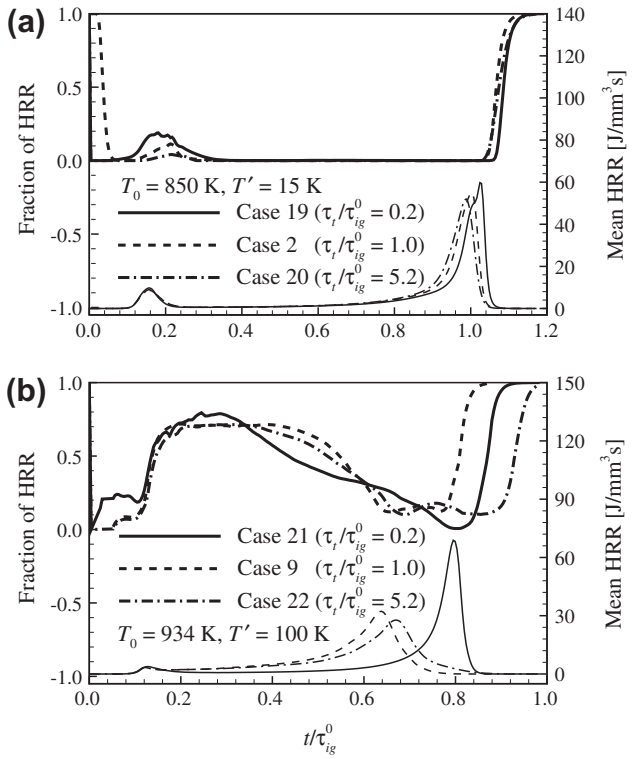

Fig. 22. Temporal evolution of fraction of heat release rate from the deflagration mode (thick lines) and heat release rate (thin lines) with different τ_t: (a) T_0 = 850 K with T' = 15 K and (b) T_0 = 934 K with T' = 100 K.

longer τ_t, a considerable fraction of $\dot{q}$ by the deflagration mode persists for a longer duration beyond the peak of $\bar{\dot{q}}$. Together with the temperature fluctuation behavior shown in Fig. 21, these results verify that the non-monotonicity in the ignition delay is attributed to the change of combustion mode according to the ratio of the turbulence timescale to the ignition delay; i.e., mixed mode combustion enhances the overall combustion to a greater extent than pure deflagration (large τ_t/τ_{ig}^0) or spontaneous ignition (small τ_t/τ_{ig}^0) combustion.

In summary, turbulent mixing, through its competitive role with auto-ignition generated scalar gradients, plays an important role in determining the ignition delay. Namely, turbulent mixing reduces scalar fluctuations and dissipates heat and radicals from developing ignition kernels. However, comparatively, the extent of ignition delay change and spreading of heat release rate induced by turbulence is not as great as that by T_0 and T' due to the high sensitivity to temperature of Arrhenius chemical reactions.

6. Conclusions

The effects of thermal stratification (through both mean and fluctuations in initial temperature) and turbulent mixing timescales on auto-ignition of a lean homogeneous *n*-heptane/air mixture at constant volume and high pressure are investigated by direct numerical simulations with a new 58-species reduced *n*-heptane/air kinetic mechanism. In the first parametric study, the homogeneous ignition delay was held constant, and twelve cases with varying initial mean temperature straddling the NTC regime were studied with different degrees of temperature fluctuations imposed. The displacement speed, Damköhler number, and chemical explosive mode analyses verify that, in general, larger T' induces greater temporal spreading of the mean heat release rate because the deflagration mode is predominant at the reaction fronts for large T'. However, spontaneous ignition prevails for small T', and hence, simultaneous auto-ignition occurs throughout the whole domain, resulting in an excessive rate of pressure rise. For mean temperatures lower than the NTC regime, e.g. with $T_0 = 850$ K, the ignition delay is increased with increasing T'. On the contrary, the ignition delay is significantly decreased with T' for mean temperatures greater than the NTC region (e.g. $T_0 = 1008$ K). For mean temperatures within the NTC region, e.g. with $T_0 = 934$ K, the combined effects of high and low temperature manifest themselves such that the ignition delay is increased for small T' but is advanced with large T'.

In the second parametric study, the homogeneous ignition delays were halved and doubled for cases with $T_0 = 1067$ K and $T_0 = 754$ K, respectively. For the cases with high $T_0 = 1067$ K, the ignition delay is significantly decreased and the temporal spreading of the mean heat release rate is also enhanced with increasing T', similar to the cases with $T_0 = 1008$ K. For cases with low $T_0 = 754$ K, however, the ignition delay and temporal spreading of the mean heat release rate are not significantly affected by thermal stratification. This is because the turbulence timescale (=2.49 ms) is short relative to the second-stage ignition delay time, and hence, thermal fluctuations are homogenized by fast mixing prior to the second-stage ignition. Therefore, the second-stage ignition is not significantly affected by turbulence.

Finally, in the third parametric study the ratio of the turbulence to ignition delay timescale was also found to change the ignition characteristics of the mixtures. A fast turbulence timescale is able to homogenize the mixture such that ignition is more apt to occur by spontaneous ignition for both large and small T' cases. Longer turbulence timescales, however, are not able to homogenize temperature fluctuations prior to thermal runaway. Therefore, for cases with small T', ignition occurs independently in each ignition kernel, and for cases with large T', ignition occurs primarily by deflagration, resulting in a smooth mean heat release rate. Overall, the effect of different turbulence timescales on the ignition delay is small compared with that of thermal stratification.

These results imply that the critical degree of thermal stratification for smooth operation of HCCI engines depends on both the mean initial temperature and the level of fluctuations. Therefore, tailoring both mean and fluctuations of initial temperature should be considered to control both HCCI ignition timing and to prevent an excessive rate of pressure rise.

Acknowledgments

The work at Ulsan National Institute of Science and Technology (UNIST) was supported by the 2009 Research Fund of UNIST. The work at University of Connecticut was supported by the National Science Foundation under Grant No. 0904771. Any opinions, findings, and conclusions or recommendations expressed in this material are those of the authors and do not necessarily reflect the views of the National Science Foundation. The work at Sandia National Laboratories (SNL) was supported by the Division of Chemical Sciences, Geosciences, and Biosciences, Office of Basic Energy Sciences, and Office of Advanced Scientific Computing Research of the US Department of Energy. JHC was also supported as part of the Combustion Energy Frontier Research Center, an Energy Frontier Research Center funded by the US Department of Energy, Office of Science, Office of Basic Energy Sciences under Award Number DE-SC0001198. SNL is a multiprogram laboratory operated by Sandia Corporation, a Lockheed Martin Company, for the US Department of Energy under contract DE-AC04-94AL85000. The work at Princeton University was supported by the Air Force Office of Scientific Research under the technical monitoring of Dr. Julian M. Tishkoff, and by the Combustion Energy Frontier Research Center sponsored by the US Department of Energy.

Appendix A. Supplementary data

Supplementary data associated with this article can be found, in the online version, at doi:10.1016/j.combustflame.2011.01.025.

References

[1] J.E. Dec, Proc. Combust. Inst. 32 (2009) 2727–2742.
[2] M. Yao, Z. Zheng, H. Liu, Prog. Energy Combust. Sci. 35 (2009) 398–437.
[3] J.A. Eng, SAE Paper 2002–01–2859, 2002.
[4] A. Hultqvist, M. Christenson, B. Johansson, M. Richter, J. Nygren, J. Hult, M. Alden, SAE Paper 2002–01–0424, 2002.
[5] A. Babajimopoulos, G.A. Lavoie, D.N. Assanis, SAE Paper 2003–01–3220, 2003.
[6] D. Reuss, V. Sick, SAE Trans. Paper 2005–01–2122, 2005.
[7] J.E. Dec, W. Hwang, M. Sjöberg, SAE Trans. Paper 2006–01–1518, 2006.
[8] M. Sjöberg, J.E. Dec, SAE Trans. Paper 115, 2006, pp. 318–334.
[9] J.E. Dec, W. Hwang, SAE Trans. Paper 2009–01–0650, 2009.
[10] M. Richter, J. Engström, A. Franke, M. Aldén, A. Hultqvist, B. Johansson, SAE Trans. Paper 2000–01–2868, 2000.
[11] J.E. Dec, M. Sjöberg, SAE Trans. Paper 112 2003–01–0752, 2003.
[12] R.R. Steeper, S.D. Zilwa, SAE Paper 2007–01–0180, 2007.
[13] P.W. Aroonsrosopon, P. Werner, J.O. Waldman, SAE Tran. Paper 113 2004–01–1756, 2004.
[14] W. Hwang, J.E. Dec, M. Sjöberg, SAE Trans. Paper 116 2007–01–4130, 2007.
[15] H. Nordgren, A. Hultqvist, B. Johansson, SAE Trans. Paper 2005–01–2990, 2004.
[16] J. Hyvönen, G. Haraldsson, B. Johansson, SAE Paper 2005–01–0109, 2005.
[17] H. Persson, A. Hultqvist, B. Johanass, A. Remón, SAE Paper 2007–01–0212, 2007.
[18] R. Sankaran, H.G. Im, E.R. Hawkes, J.H. Chen, Proc. Combust. Inst. 30 (2005) 875–882.
[19] J.H. Chen, E.R. Hawkes, R. Sankaran, S.D. Mason, H.G. Im, Combust. Flame 145 (2006) 128–144.
[20] E.R. Hawkes, R. Sankaran, P. Pébay, J.H. Chen, Combust. Flame 145 (2006) 145–159.
[21] Y.B. Zeldovich, Combust. Flame 39 (1980) 211–214.
[22] S. Liu, J.C. Hewson, J.H. Chen, H. Pitsch, Combust. Flame 137 (2004) 320–339.
[23] S. Liu, J.C. Hewson, J.H. Chen, Combust. Flame 145 (2006) 730–739.
[24] G. Bansal, H.G. Im, S.R. Lee, Proc. Combust. Inst. 32 (2009) 1083–1090.

[25] H.G. Im, J.H. Chen, C.K. Law, Proc. Combust. Inst. 27 (1998) 1047–1056.
[26] T. Echekki, J.H. Chen, Combust. Flame 134 (2003) 169–191.
[27] S. Tanaka, F. Ayala, J.C. Keck, J.B. Heywood, Combust. Flame 132 (2003) 219–239.
[28] X. Lü, L. Ji, L. Zu, Y. Hou, C. Huang, Z. Huang, Combust. Flame 149 (2007) 261–270.
[29] A. Dubreuil, F. Foucher, C. Mouaïm-Rousselle, G. Dayma, P. Dagaut, Proc. Combust. Inst. 31 (2007) 2886–2897.
[30] G. Bogin Jr., J.-Y. Chen, R.W. Dibble, Proc. Combust. Inst. 32 (2009) 2877–2884.
[31] D.A. Rothamer, J.A. Snyder, R.K. Hanson, R.R. Steeper, R.P. Fitzgerald, Proc. Combust. Inst. 32 (2009) 2869–2876.
[32] T. Lu, C.K. Law, Combust. Flame 144 (2006) 24–36.
[33] H.J. Curran, P. Gaffuri, W.J. Pitz, C.K. Westbrook, Combust. Flame 114 (1998) 149–177.
[34] H.J. Curran, P. Gaffuri, W.J. Pitz, C.K. Westbrook, Combust. Flame 129 (2002) 253–280.
[35] T. Lu, C.K. Law, Combust. Flame 154 (2008) 153–163.
[36] T. Lu, C.K. Law, C.S. Yoo, J.H. Chen, Combust. Flame 156 (2009) 1542–1551.
[37] R. Sankaran, E.R. Hawkes, J.H. Chen, T. Lu, C.K. Law, Proc. Combust. Inst. 31 (2007) 1291–1298.
[38] X.L. Zheng, T. Lu, C.K. Law, Proc. Combust. Inst. 31 (2007) 367–375.
[39] T. Lu, C.K. Law, Combust. Flame 154 (2008) 761–774.
[40] T. Lu, C.K. Law, J. Phys. Chem. A 110 (2006) 13202–13208.
[41] T. Lu, C.K. Law, Combust. Flame 148 (2007) 117–126.
[42] A.E. Lutz, R.J. Kee, J.A. Miller, SENKIN: A Fortran Program for Predicting Homogeneous Gas Phase Chemical Kinetics with Sensitivity Analysis, Tech. Rep. SAND87-8248, Sandia National Laboratories, 1987.
[43] R.J. Kee, J.F. Grcar, M.D. Smooke, J.A. Miller, A Fortran Program for Modeling Steady Laminar One-dimensional flames, Tech. Rep. SAND85-8240, Sandia National Laboratories, 1985.
[44] J.H. Chen, A. Choudhary, B. de Supinski, M. DeVries, E.R. Hawkes, S. Klasky, W.K. Liao, K.L. Ma, J. Mellor-Crummey, N. Podhorszki, R. Sankaran, S. Shende, C.S. Yoo, Comput. Sci. Disc. 2 (2009) 015001.
[45] C.A. Kennedy, M.H. Carpenter, Appl. Numer. Math. 14 (1994) 397–433.
[46] C.A. Kennedy, M.H. Carpenter, R.M. Lewis, Appl. Numer. Math. 35 (2000) 117–219.
[47] R.J. Kee, F.M. Rupley, E. Meeks, J.A. Miller, CHEMKIN-III: A Fortran Chemical Kinetic Package for the Anaylsis of Gas-phase Chemical and Plasma Knietics, Tech. Rep. SAND96-8216, Sandia National Laboratories, 1996.
[48] R.J. Kee, G. Dixon-Lewis, J. Warnatz, M.E. Coltrin, J.A. Miller, A Fortran Computer Code Package for the Evaluation of Gas-phase Multicomponent Transport Properties, Tech. Rep. SAND86-8246, Sandia National Laboratories, 1986.
[49] T. Passot, A. Pouquet, J. Fluid Mech. 118 (1987) 441–466.
[50] C.S. Yoo, Y. Wang, A. Trouvé, H.G. Im, Combust. Theory Model. 9 (2005) 617–646.
[51] C.S. Yoo, H.G. Im, Proc. Combust. Inst. 31 (2007) 701–708.
[52] E.R. Hawkes, J.H. Chen, Combust. Flame 138 (2004) 242–258.
[53] C.K. Law, Combustion Physics, Cambridge University Press, 2006.
[54] C.H. Gibson, Phys. Fluids 11 (1968) 2305–2315.
[55] T. Echekki, J.H. Chen, Combust. Flame 118 (1999) 308–311.
[56] C.S. Yoo, H.G. Im, Proc. Combust. Inst. 30 (2005) 349–356.
[57] C.S. Yoo, J.H. Chen, J.H. Frank, Combust. Flame 156 (2009) 140–151.
[58] C.S. Yoo, R. Sankaran, J.H. Chen, J. Fluid Mech. 640 (2009) 453–481.
[59] C.S. Yoo, E.S. Richardson, R. Sankaran, J.H. Chen, Proc. Combust. Inst. 33 (2011) 1619–1627.
[60] T. Lu, C.S. Yoo, J.H. Chen, C.K. Law, J. Fluid Mech. 652 (2010) 45–64.
[61] T. Lu, C.S. Yoo, J.H. Chen, The role of chemical explosive mode in flames, in: Fall Technical Meeting, the Eastern Section Meeting of the Combustion Institute, College Park, USA, 2009.